Available online at www.sciencedirect.com
ScienceDirect
Deep-Sea Research II 55 (2008) 126–136
DEEP-SEA RESEARCH PART II
www.elsevier.com/locate/dsr2

Deep-sea pelagic bioluminescence over the Mid-Atlantic Ridge

A. Heger[a,*], E.N. Ieno[a,b], N.J. King[a], K.J. Morris[a], P.M. Bagley[a], I.G. Priede[a]

[a]*Oceanlab, University of Aberdeen, Main Street, Newburgh, Aberdeenshire AB41 6AA, UK*
[b]*Highland Statistics Ltd., 6 Laverock Road, Newburgh, Aberdeenshire AB41 6FN, UK*

Accepted 13 September 2007
Available online 21 December 2007

Abstract

Measurements were made for the first time of the number of stimulated sources of bioluminescence from the subsurface layer to the seafloor at 14 stations over the northern Mid-Atlantic Ridge, 42°56′N to 53°18′N. Overall, light emissions decreased from typical means of 46 sources m^{-3} at 300–500 m down to 5 m^{-3} at 2800 m depth. In the vicinity of the Azores, higher mean abundance (29.4 m^{-3}) occurred at 500–1500 m compared to 13.9 m^{-3} over the same depth range at a reference station east of the ridge. Compared with the reference station, elevated levels of bioluminescence (25 m^{-3}) were also observed at depths of 700–965 m in the water column over the Faraday Seamount. North of the Subpolar Front there was little variability in the number of bioluminescent sources between the sampling stations. However, in the Frontal Zone high abundance of bioluminescent sources was detected down to 1500 m within an anticyclonic eddy. Smoothing techniques revealed that >90% of the observed variation in the distribution of bioluminescence over the ridge was explained by sample depth in the water column.

Keywords: Bioluminescence; Deep-sea; Vertical distribution; Seamounts; Mesoscale eddy; Mid-Atlantic Ridge

1. Introduction

A high proportion of pelagic species are bioluminescent and it is reasonable to assume that the spatial and temporal variability of bioluminescence will reflect changes in the abundance and distribution of pelagic biota/biomass (Piontkovski et al., 1997). Measurements of light emission potential in the oceans generally have been made using mechanical stimulation to induce bioluminescence in marine organisms. Such sampling has mostly been restricted to the epipelagic zone, but deep vertical profiles using bathyphotometers have been obtained in the Northwest Atlantic down to a depth of 3750 m (Clarke and Hubbard, 1959; Clarke and Kelly, 1965) and in the Pacific off Hawaii between 500 and 4300 m (Bradner et al., 1987; Webster et al., 1991). In the Gulf of Maine and Monterey Bay Canyon, video observations of organisms impacting were achieved using manned submersibles <1000 m depth (Widder et al., 1989; Widder and Johnsen, 2000). Using the mesh screen detection principle on a free-fall lander system, Priede et al. (2006) obtained bioluminescence profiles in the vicinity of the Cape Verde Islands off west Africa between 500 and 4046 m depth, and Gillibrand et al. (2007) profiled the water column to depths of 4800 m in the Porcupine Seabight and Abyssal Plain regions in the Northeast Atlantic.

Here we report the first observations of stimulated bioluminescent pelagic organisms from the surface down to the seafloor at stations along and across the Mid-Atlantic Ridge (MAR) using the impact screen method in tandem with CTD profiling. The MAR is the dominant physiographic feature in the North Atlantic, characterized by complicated topography with depths ranging from 4500 m in the deepest channel to 700–800 m on top of adjacent seamounts. The topography of the MAR affects the circulation pattern of different water masses in the North Atlantic (Rossby, 1999; Bower et al., 2002). At 52–53°N, the axis of the MAR is distorted by the Charlie–Gibbs Fracture Zone (CGFZ) and it is in that region, in the surface waters, that the North Atlantic Current crosses the MAR from west to east defining a boundary, the Subpolar Front (SPF) (also called the Subarctic Front), between cold

*Corresponding author. Tel.: +44 1224 274401; fax: +44 1224 274402.
E-mail address: a.heger7@gmail.com (A. Heger).

0967-0645/$ - see front matter © 2007 Elsevier Ltd. All rights reserved.
doi:10.1016/j.dsr2.2007.09.014

low-salinity waters to the north, Subarctic Intermediate Water (SAIW), and warm saline waters to the south, North Atlantic Central Water (NACW) (Sy et al., 1988, 1992; Rossby, 1999). Detailed descriptions of the circulation and the relevant water masses in this region of the North Atlantic can be found in the paper by Søiland et al. (2008).

The intricate hydrographic setting and the presence of the MAR leads to enhanced vertical mixing and turbulence (Mauritzen et al., 2002) resulting in areas of increased productivity over the MAR (Falkowski et al., 1998), which may in turn support enhanced pelagic biomass and abundance of bioluminescent organisms. In this study we compare the abundance and vertical distribution of bioluminescent organisms at different latitudes east and west of the MAR in order to understand the influence of the MAR system and its associated hydrographic regime on pelagic organisms. Special attention is given to two clusters of stations, one situated north of the SPF (northwest of the CGFZ) and another one located within the SPF zone (southeast of the CGFZ).

2. Materials and methods

2.1. Data collection

Data were collected in the summer of 2004 (4 July–5 August) during leg 2 of the voyage of the R.V. *G.O. Sars* between the Azores and Iceland (Wenneck et al., 2008). A free-fall bioluminescence recording system, described by Priede et al. (2006), was integrated with the ship's CTD (SBE 911plus)/water bottle rosette profiling system in a downward-looking orientation. An Intensified Silicon Intensifier Target (ISIT) camera (OE1325: Kongsberg Simrad, UK, faceplate sensitivity 5×10^{-6} lx) was used as the bioluminescence detector. Two water-sampling bottles were removed from the CTD rosette to allow for this modification. A 380×500-mm mesh screen with an 8×16-mm pitch was mounted to the base of the CTD frame in the centre of the field of view 800 mm below the ISIT camera. As the ISIT-CTD profiling system was lowered through the water column any potentially bioluminescent organisms impacting on, or passing through the mesh screen were mechanically stimulated and light output detected by the ISIT camera was recorded with a miniature digital video (DV) recorder (Walkman GV-D300; Sony, Japan) controlled via a pre-programmed 68,000 base microprocessor (Onset Computer Corp., USA). A 20-W underwater light (Deep Multi-Lite; DSPL Inc., USA) illuminating the field of view of the ISIT camera was programmed to flash once at a predetermined time in order to synchronize the ISIT to the ship's clock. Depth, temperature, salinity, oxygen and fluorescence levels were acquired using the standard instruments on the CTD as the instrument descended at a nominal speed of $0.8\,m\,s^{-1}$ on the winch cable. At this descent rate, continuous recording was possible over 2880 m of depth at 25 frames s^{-1} during 60-min duration of the DV tape.

2.2. Deployment sites

The ISIT-CTD bioluminescence profiler was deployed at 14 "SuperStations" (SS) distributed across the MAR (Fig. 1). Single deployments were conducted north of the Azores at 42°N (SS52, 'southern' station hereafter) and at the Faraday Seamount (SS53) (49°N). Six deployments, SS54–64, were undertaken southeast of the CGFZ (51°N) in the SPF, an area we define here as the "Frontal Zone", and six stations, SS66–76, were profiled northwest of the CGFZ (53°N) in the region defined as "North of the Front" (Table 1). Depths ranged from 1012 m at the summit of the Faraday Seamount to 3477 m at a station east of the ridge (SS54). Sampling with the ISIT-CTD profiler was conducted down to an altitude of 10–708 m off the seafloor.

2.3. Data extraction

All videos from the ISIT-CTD profiler deployments were viewed frame-by-frame using proprietary software (Final Cut Pro, v2.0, Apple Computers Inc., USA) and the number of bioluminescent events per 30 s was counted. Using the known mesh area and descent rate of the CTD rosette these data were converted to the number of bioluminescent sources per m^3 at approximately 24-m depth intervals (these varied slightly owing to small changes in winch speeds). Counting was not possible at depths shallower than 300 m due to ambient light. A bioluminescent event was recorded at the time of initial interaction with the mesh screen. Multiple flashes resulting from disintegration of an organism (or colonial organisms) or sequential pulses from an organism trapped on the screen were all counted as a single source representing one luminescent organism.

In order to graphically present the relationship of the bioluminescence with the bottom topography of the ridge, contour plots of vertical sections North of the Front and in the Frontal Zone were generated using Surfer® Software (Golden Software Inc., USA) with the x-axis as distance (km) from east to west.

2.4. Statistical analysis

The relationship between the abundance (number of sources m^{-3}) of pelagic bioluminescent organisms and environmental variables was analysed using additive modelling (Hastie and Tibshirani, 1990; Faraway, 2006; Zuur et al., 2007). This smoothing method was applied because preliminary analyses using a linear regression model showed that the relationship between response (sources m^{-3}) and explanatory variables (environmental factors, e.g. depth) was non-linear. In order to choose the optimal amount of smoothing (degrees of freedom), cross-validation was used (Wood, 2006).

Prior to analysis, graphical explanatory techniques (boxplots and Cleveland dotplots) (Cleveland, 1993) were

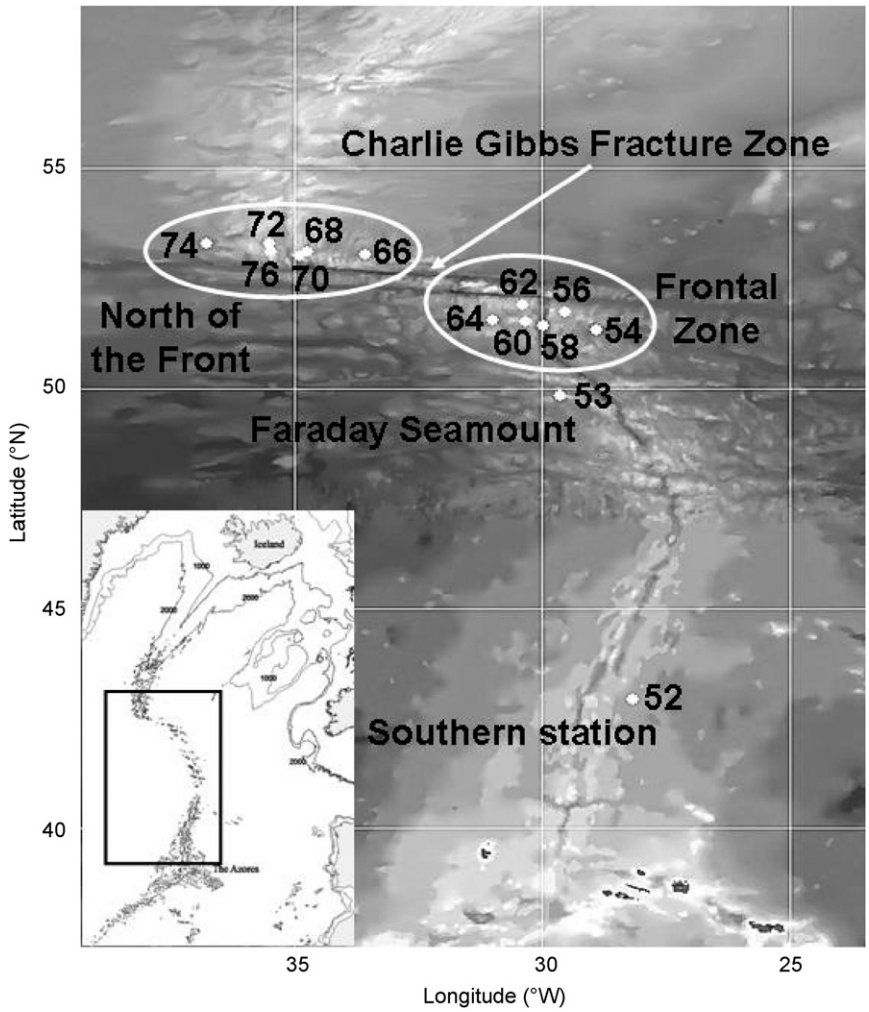

Fig. 1. Map of study area showing the section of the Mid-Atlantic Ridge (MAR) under investigation. The ISIT-CTD profiling SuperStations (SS52–76) are shown along and across the ridge from leg 2 of the voyage of the R.V. *G.O. Sars*.

Table 1
Deployment details for the ISIT-CTD bioluminescence profiler during the 2004 R.V. *G.O. Sars* Mid-Atlantic Ridge expedition (North Atlantic Ocean)

SS	Latitude (N)	Longitude (W)	Location	Generic term	Sounding depth (m)	Date	Start time	Solar cycle
52	42°56.02′	28°09.13′	East end of southern transect	Southern station	2973	13 July	6:29	Day
53	49°50.99′	29°36.90′	Faraday Seamount	Faraday Seamount	1012	15 July	21:01	Dusk
54	51°20.56′	28°53.52′	First station east end of mid transect	Frontal Zone (south of the CGFZ) SS54 is also referred to as reference station	3477	16 July	6:43	Day
56	51°45.29′	29°32.07′	On rise of east side of ridge		1890	17 July	2:55	Night
58	51°25.42′	29°58.01′	In mid rift valley		3342	17 July	19:40	Day
60	51°31.71′	30°19.04′	On crest peak, west side of ridge		1100	18 July	20:17	Day
62	51°53.79′	30°23.72′	West of ridge		1697	19 July	16:16	Day
64	51°32.58′	30°59.62′	West end of transect		3462	20 July	22:18	Night
66	53°02.55′	33°33.47′	First station north of CGFZ	North of the Front (north of the CGFZ)	3067	24 July	7:53	Day
68	53°07.43′	34°44.80′	Flank of east ridge		2144	25 July	5:20	Night
70	53°00.26′	34°54.94′	Crest of east ridge		1748	26 July	23:01	Night
72	53°18.15′	35°30.58′	Median valley area		2435	27 July	5:36	Night
74	53°17.55′	36°46.04′	West of ridge		3059	27 July	22:11	Day
76	53°05.96′	35°28.18′	Crest of west ridge		1243	29 July	0:58	Night

SS: SuperStation; start time in UTC (hh:mm); CGFZ: Charlie–Gibbs Fracture Zone.

applied to the original data to identify outliers both in the response variable and the explanatory variables. Correlation between explanatory variables (collinearity) was assessed by multiple pair-wise scatter plots (pair plots).

All statistical analyses were performed using the software package Brodgar 2.5.2 (www.brodgar.com) and R (www.r-project.org) using the mgcv R library (Wood, 2006; R Development Core Team, 2006).

3. Results

3.1. Bioluminescent sources

Bioluminescence was detected at all stations and displayed a general decrease in abundance with depth. Fig. 2 provides examples of bioluminescent sources observed in the water column at various stations and depths. In the top layers (300–700 m), the bioluminescent signatures consisted mainly of a multitude of single flashes or short trails of light (<1 s) that were likely produced by small pelagic animals as they passed through the screen (Fig. 2A–C). In the mid-layers (700–2000 m), as the number of small events decreased, larger luminescent displays from gelatinous organisms formed a conspicuous component of the stimulated bioluminescence and a number of them were identified as chain-forming siphonophores (Fig. 2D) or medusae (Fig. 2F), possibly *Atolla wyvillei* (Herring and Widder, 2004). Occasionally, organisms would become trapped on the screen and emit intense light at repeated intervals (for up to several minutes) until they disintegrated or exhausted their light potential (Fig. 2E). At deeper depths (2000 m to the seafloor), small flashes became less frequent (Fig. 2G and H) and sporadic larger events were still present (Fig. 2I).

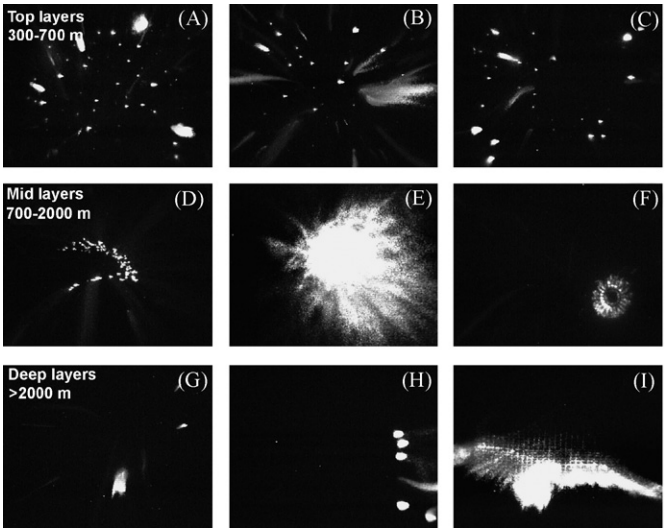

Fig. 2. Single video frames illustrating different abundance and shapes of bioluminescent organisms at various stations and depths. Examples of single flashes (probably produced by small crustaceans) are shown in the top layers at (A) SS62: 323 m, (B) SS76: 340 m, (C) SS53: 505 m; gelatinous zooplankton signals are shown for the mid layers at (D) SS68: 780 m (chain-forming organism, probably a siphonophore), (E) SS76: 810 m, (F) SS64: 845 m (a medusa, possibly *A. wyvillei*; Herring and Widder, 2004); large emissions are shown for the deep layers at (G) SS52: 2000 m, (H) SS54: 2335 m, (I) SS66: 2535 m (fragile organisms disintegrated by the screen). The size of the images corresponds to the dimensions of the mesh screen (380 × 500 mm).

3.2. Comparison of Frontal Zone, seamount and southern stations

Representative plots of original data and corresponding temperatures from contrasting geographical locations are shown in Fig. 3. SS54, a deep station located east (ca. 111 km) of the ridge and south of the CGFZ, exhibited an open-ocean profile, and for purpose of discussion, SS54 was used as a reference station away from any potential influence of topography. This station had a mean of 46 sources m^{-3} above 500 m, 14 m^{-3} at 500–1500 m and 6 m^{-3} between 1500 m and the seafloor (Fig. 3A). Water temperature also decreased with depth from a mean of 7.2 °C above 500 m to 3.1 °C between 1500 m and the seafloor. Further south at SS53 (Fig. 3B), over the Faraday Seamount, temperature and abundance of bioluminescent organisms followed a similar pattern with a mean of 51 m^{-3} above 500 m, but in the water column immediately above the summit the abundance was 25 m^{-3} between 700 and 965 m compared to 13 m^{-3} over the same depth interval at SS54. The water temperature at SS53 was slightly lower than at SS54 (mean $T = 6.8$ °C above 500) and at deeper depths, 500–1000 m, temperatures were similar at both stations (mean $T = 4$ °C). Salinity was constant at 34.9 at comparable depths. Just North of the Azores, the southern station (SS52) (Fig. 3C), located in warmer waters and higher surface salinities (mean $T = 13.9$ °C, $S = 35.8$ above 500 m), had lower concentrations of bioluminescence (mean of 39 sources m^{-3}) above 500 m but elevated abundance (29 m^{-3}) (double that at SS54) in deeper waters at 500–1500 m ($T = 7.1$ °C) and 8 m^{-3} ($T = 3.5$ °C) between 1500 m and the seafloor.

3.3. North of the Front

Contour plots were created in order to visualize the distribution of bioluminescence both North of the Front and in the Frontal Zone (Fig. 4). North of the Front (Fig. 4A), all six stations (SS66–76) seemed to exhibit a similar and constant decrease with depth from an average of 47 sources m^{-3} above 500 m, to 12 m^{-3} between 500 and 1500 m and 4 m^{-3} from 1500 m to the seafloor for the deep profiles. Water temperatures and salinities at all stations were relatively similar ($T = 6$–7 °C, $S < 34.9$ in the top 500 m). The highest abundance of bioluminescence sources (peak of 128 sources m^{-3}) throughout this study was found in the top layers at SS70.

3.4. Frontal Zone

The hydrographic regime of the Frontal Zone (SS54–64) was complex and profiles revealed elevated biolumines-

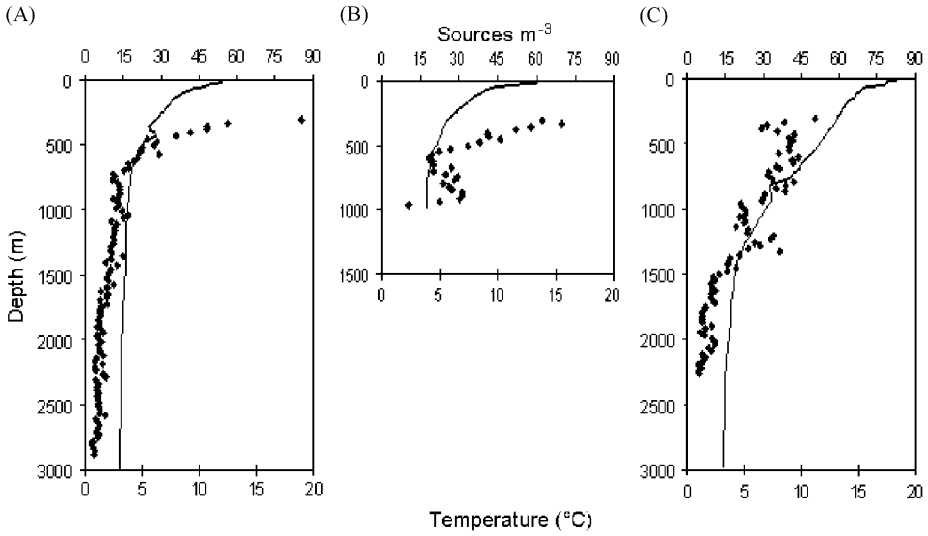

Fig. 3. Scatter plots of bioluminescent sources m^{-3} as a function of depth for (A) reference station (SS54), (B) Faraday Seamount (SS53) and (C) southern station (SS52). Each point is derived from a count during 30 s of descent through the water column corresponding to a ca. 24-m depth change. The corresponding temperature data from the CTD are depicted by a solid line.

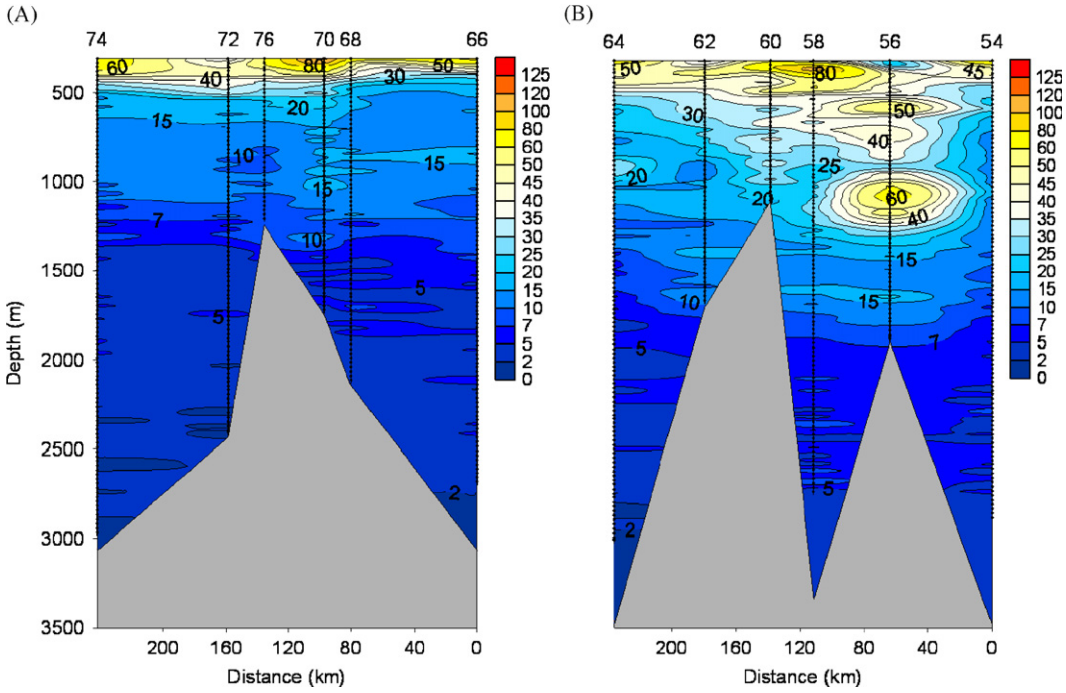

Fig. 4. Contour plots of bioluminescence abundance as a function of depth (m) and distance (km) across the Mid-Atlantic Ridge (MAR) for (A) North of the Front (SS66–76) and (B) Frontal Zone (SS54–64). Numbers along the top of the contour plot represent SuperStation (SS) numbers. The distance scale is based on incremental calculated great circle straight line lengths between station locations with zero as the eastern-most station. The profile of the MAR is indicated by the polygon bounded by straight lines between the depth soundings at each station. The depth of each ISIT-CTD cast is indicated by the vertical dotted line.

cence abundance at most stations and depths (Fig. 4B). Above 500 m a mean of 50 sources m^{-3} was detected, decreasing to 24 m^{-3} between 500 and 1500 m and reached a minimum (mean of 8 sources m^{-3}) between 1500 m and the seafloor. SS56, 58, 60 and 62 were found to be within the zone of influence of a warm anticyclonic eddy, characterized by a strong temperature/salinity signal down to about 700 m depth (Søiland et al., 2008). Those stations showed a distinct enhancement of deep bioluminescent activity (by a factor of two) between 500 and 1500 m compared to SS54 and SS64 (mean of 29 vs. 15 sources m^{-3}), which were found to be outside the eddy in colder, fresher waters. The deeper profile situated in the mid-rift valley (SS58) also showed higher abundance between 1500 m and the bottom compared to SS54 and SS64 (8 vs. 5 sources m^{-3}). On the eastern side of the ridge

crest, SS56 in particular exhibited elevated deep bioluminescence with a mean of 40 sources m^{-3} above 500 m and 13 m^{-3} between 1500 m and the seafloor.

3.5. Additive modelling

After initial analysis of the data, a square-root transformation was applied to the response variable (sources m^{-3}) to reduce the effect of outliers (extreme large observations). Pairplots of the continuous variables for each station indicated strong collinearity namely between depth, temperature, salinity and oxygen concentration. Nominal variables such as "day/night" and "station" were confounding and thus not considered in the analysis. *In situ* fluorescence was not collinear but was found to have no significant effect ($p>0.05$) in any of the models describing the depth profiles. Therefore, for analytical purposes only depth was used as the putative explanatory variable.

Additive modelling was applied to each station, producing the formula:

$$\sqrt{(sources_i)} = \alpha + f(Depth_i) + \varepsilon_i,$$

where $\sqrt{(sources_i)}$ was the square-root transformed abundance (bioluminescent sources m^{-3}) for observation i, and was modeled as a smoothing function of depth, an intercept α and the residual ε_i (unexplained information or noise, $\varepsilon_i \sim N(0,\sigma^2)$). The R^2 values (explained amount of variation = deviance) (Wood, 2006) for all models were >0.90, indicating that $>90\%$ of the observed variation in bioluminescence was explained by depth.

In order to test whether two stations had the same sources-depth patterns, we applied the following two-nested models:

$$\sqrt{(sources_i)} = \alpha + f(Station) + f(Depth_i) + \varepsilon_i, \quad \text{(M1)}$$

$$\sqrt{(sources_i)} = \alpha + f(Station) + f_1(Depth_i) : S_1 + f_2(Depth_i) : S_2 + \varepsilon_i. \quad \text{(M2)}$$

In (M1), one smoothing curve for both stations was used. In (M2), the notation $f_1(Depth_i) : S_1$ means that the smoothing was based on data for one station only. Hence each station was allowed to have its own smoother. A likelihood ratio test was applied as both models were nested (Wood, 2006). Technically, (M2) was fitted using the "by" command in the GAM function (mgcv library).

The estimated smoothing curves for all stations are plotted in Fig. 5. North of the Front all stations displayed a monotonic decline in sources m^{-3} with depth, with only minor perturbations in the profiles. The stations in the Frontal Zone generally showed elevated abundances below 500 m compared with North of the Front stations, and SS56, located within an eddy, exhibited a peak of abundance at 1200 m. SS53 at the Faraday Seamount also showed a clear peak in abundance at about 900 m depth, an altitude of 100 m above the summit of the seamount. The southern-most SS52 had low abundance near the surface,

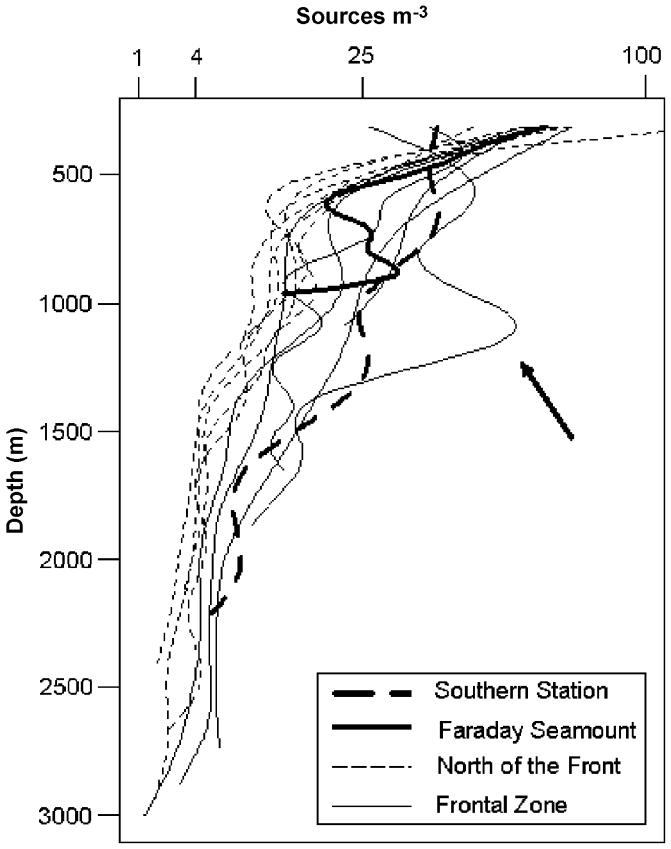

Fig. 5. Fitted smoother values obtained by additive modelling for each station. Thick dashed line represents the southern station (SS52), thick solid line represents the Faraday Seamount station (SS53), thin dotted lines represent North of the Front stations (SS66–76), thin solid lines represent Frontal Zone stations (SS54–64). Arrow indicates SS56. The horizontal axis equals sources m^{-3} plotted on a square-root scale.

lower rate of decrease with depth and elevated values at depth compared with more northerly stations.

3.5.1. Comparison of Frontal Zone, seamount and southern stations

Additive modelling revealed significant differences ($p<0.001$) between SS52, 53 and 54, both in terms of absolute abundance (sources m^{-3}) and depth distribution, between a comparable depth interval of 300–1000 m (Table 2; Fig. 6). The southern station (SS52) had a considerably ($p<0.001$) higher abundance of bioluminescence compared to the Faraday Seamount (SS53) and the latter station showed a significant ($p<0.001$) increase in bioluminescence compared to the reference station (SS54).

3.5.2. North of the Front

The smoother station interaction approach as described in Eq. (M2) was applied on sources-depth profiles for all stations. In terms of abundance, additive modelling revealed that overall SS68 and SS70 had a significantly ($p<0.001$) higher number of luminescent sources m^{-3} than SS66, whereas the other stations (SS72, 74, and 76) showed similar trends to SS66 (Table 2). Despite the fact that

Table 2
Synopsis of the additive modelling analyses

	Abundance[a]					Depth distribution			
	Estimate	Standard err.	*t*-value	*p*-value		Edf	*F*	R^2	*p*-value
Regional comparison (SS52, SS53 and SS54)									
Intercept	6.00	0.05	117.3	<0.001	s(depth)SS52	8.50	11.34	0.95	<0.001
Factor(SS53)	−0.54	0.07	−7.32	<0.001	s(depth)SS53	8.42	53.34		<0.001
Factor(SS54)	−1.28	0.07	−17.68	<0.001	s(depth)SS54	6.08	89.76		<0.001
North of the Front (SS66, SS68, SS70, SS72, SS74 and SS76)									
Intercept	4.12	0.04	91.79	<0.001	s(depth)SS66	7.24	106.24	0.97	<0.001
Factor(SS68)	0.16	0.06	2.47	0.01	s(depth)SS68	6.19	76.93		<0.001
Factor(SS70)	0.73	0.06	11.56	<0.001	s(depth)SS70	7.50	194.87		<0.001
Factor(SS72)	0.1	0.06	1.56	0.12	s(depth)SS72	7.97	87.82		<0.001
Factor(SS74)	0.09	0.06	1.46	0.15	s(depth)SS74	8.32	142.53		<0.001
Factor(SS76)	−0.02	0.06	−0.24	0.81	s(depth)SS76	4.12	126.60		<0.001
Frontal Zone non-eddy stations (SS54 and SS64)									
Intercept	3.20	0.03	104.35	<0.001	s(depth)[b]	8.43	195.32	0.95	<0.001
Factor(SS64)	0.00	0.04	0.07	0.95	s(depth)SS64	7.36	12.42		<0.001
Eddy stations (SS56, SS58, SS60 and SS62)									
Intercept	6.34	0.08	75.79	<0.001	s(depth)SS56	7.50	5.95	0.85	<0.001
Factor(SS58)	−0.08	0.12	−0.70	0.48	s(depth)SS58	8.30	31.35		<0.001
Factor(SS60)	−0.17	0.12	−1.40	0.16	s(depth)SS60	2.65	15.17		<0.001
Factor(SS62)	−1.07	0.12	−9.08	<0.001	s(depth)SS62	6.75	18.65		<0.001

SS: SuperStations. The notation s(depth)SS52 refers to a smoother for SS52 data only, this is the station–depth interaction term as discussed in the methodology section. Edf is the estimated degrees of freedom for the smoothers obtained by the cross-validation method.
[a]Sources m^{-3} integrated over the whole profile.
[b]The smoother was applied to all the data.

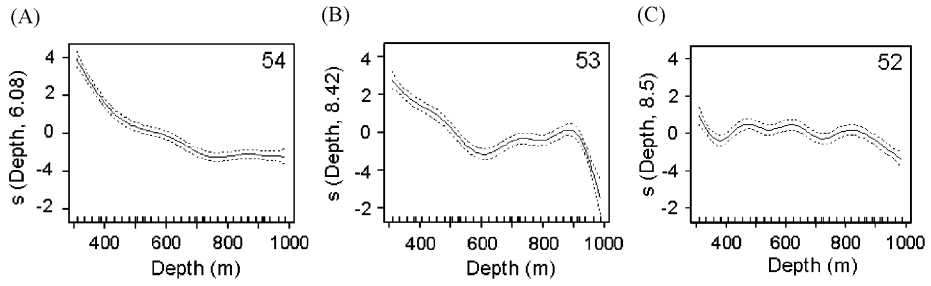

Fig. 6. Fitted smoother values for (A) reference station, SS54, (B) Faraday Seamount station, SS53, (C) southern station, SS52, down to a comparable depth of 1000 m. Vertical axis shows the contribution of smoothers to the fitted values. Dotted lines represent 95% confidence intervals.

bioluminescence profiles seemed to exhibit similar distribution with depth (see Fig. 4A), the log–likelihood ratio test revealed highly significant differences ($p<0.001$) between depth profiles for all six North of the Front stations (Table 2). They could not be statistically clustered together as similar stations (Fig. 7A) based on AIC (Akaike Information Criterion, measure of fit for model comparison; not presented here). AIC indicated that the optimal model was the one in which all the stations behaved differently over the comparable depth range of 300–1200 m.

Temperature–depth profiles for each station were analysed with the aim of explaining intra-regional variability in bioluminescence profiles. This analysis, not presented here, revealed that temperature–depth profiles of SS66, 68, 70 and 74 were the same and those of SS72 and SS76 showed a slightly different pattern. Thus bioluminescence variability between stations could not be explained hydrographically.

3.5.3. Frontal Zone

Frontal Zone stations could be characterized hydrographically into non-eddy (SS54 and SS64) and eddy groups (SS56, 58, 60 and 62). Before attempting comparisons of these two groups, within-group analyses were conducted to assess homogeneity. Analysis of the non-eddy group, down to a comparable depth of 2880 m, revealed that abundances over the whole profile at SS54 and SS64 were similar but the depth distribution of sources m^{-3} differed significantly ($p<0.001$) between both stations (Table 2), mainly in the 500–1000 m interval in which SS64 showed a different distribution (Fig. 7B).

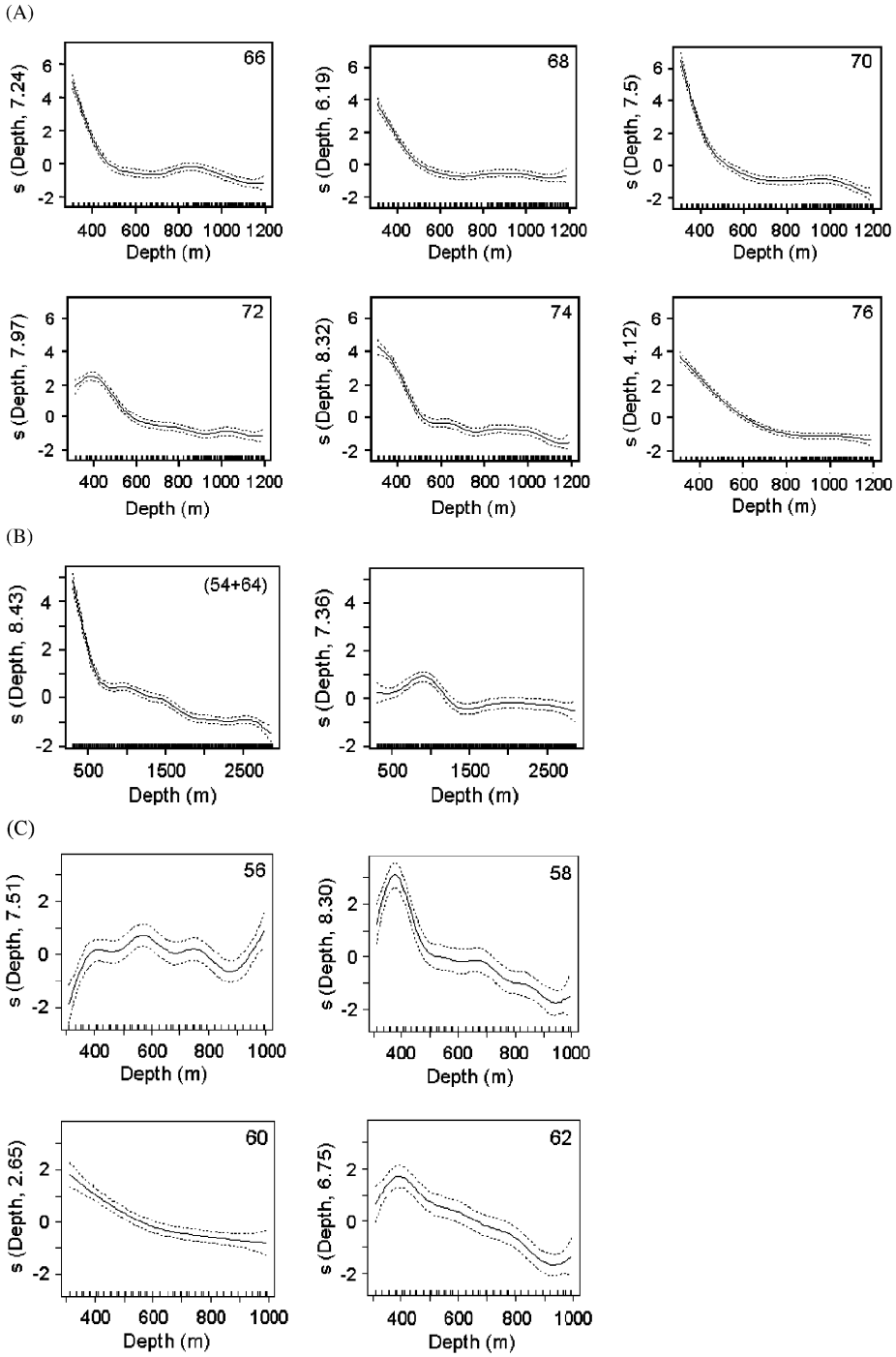

Fig. 7. Fitted smoother values for (A) North of the Front stations (SS66–76), (B) non-eddy stations (SS54 and SS64) and corresponding plot showing the deviation of SS64 from the combined data (SS54 and SS64), and (C) eddy stations (SS56–62) down to comparable depths of 1200, 2880 and 1000 m, respectively. Dotted lines represent 95% confidence intervals.

Eddy group stations (SS56–62) all displayed significantly different depth distributions ($p<0.001$) and no common patterns could be found over a comparable depth range of 1000 m (Table 2; Fig. 7C). In terms of abundance, SS56, 58 and 60 displayed a similar pattern compared to SS62 that had significantly ($p<0.001$) lower levels of bioluminescent sources.

After taking into account all stations (eddy and non-eddy stations), depth profiles were still significantly different from each other and therefore no between-group comparison was possible; again model comparisons suggested that the best way of describing profiles in the Frontal Zone was by individual curves.

3.6. Validation of models

Residuals of each station were extracted and compared with each other. Correlations of residuals of different stations were mostly smaller than 0.3 indicating that there

was no residual spatial correlation. Moreover, the residual variance for most stations in the Frontal Zone was larger compared to the North of the Front stations.

4. Discussion

4.1. Comparison with other oceanic regions

The values of the abundance of bioluminescent sources over the MAR are similar to those previously recorded in the deep Atlantic. For example, the observation of an overall decline of bioluminescence with depth coincides with other vertical profiles from the tropical Atlantic (Priede et al., 2006) and NE Atlantic (Gillibrand et al., 2007). Depth-integrated abundance in midwater (500–1500 m) was similar to that of those two previous studies with values $>20\,m^{-3}$. The abundance of bioluminescence between 1500 m and the seafloor was higher overall in this study than values at similar depths off Cape Verde (7 vs. 3 sources m^{-3}) (Priede et al., 2006). In the temperate Porcupine Seabight and Abyssal Plain area of the NE Atlantic, mean values for comparable depths were $7\,m^{-3}$ but a seasonal mean of $24.7\,m^{-3}$ was recorded in autumn profiles, compared to $7.5\,m^{-3}$ in spring deployments (Gillibrand et al., 2007).

4.2. Potential bioluminescent organisms

Although the impact screen approach does not permit identification of the light-emitting animals some shapes are recognizable, allowing one to determine groups of organisms that are being observed. The most likely candidates responsible for the majority of the displays recorded are crustacean zooplankton, such as copepods and euphausiids. On the first leg of the MAR-ECO cruise, for example, eight bioluminescent species of euphausiids were identified, including *Euphausia krohni*, *Thysanoessa longicaudata*, *Thysanopoda acutifrons* and *Meganyctiphanes norvegica*, which were the most abundant species present (Falkenhaug, personal communication). Moreover, another important fauna that could be distinguished by their luminescent signatures were gelatinous zooplankton, such as medusae. The vertical distribution and abundance of zooplankton was investigated using an underwater video profiler (UVP) and a remotely operated vehicle (ROV) at the same stations described in this study (Stemmann et al., 2008; Youngbluth et al., 2008). The dominant zooplanktonic organisms occurring throughout the water column were crustaceans, ctenophores, siphonophores, appendicularians, medusae and chaetognaths, all of which are known to have bioluminescent species (Herring, 1990). Similar organisms were also identified from recent submersible observations carried out between 170 and 4361 m in the CGFZ (Vinogradov, 2005).

4.3. Comparison of Frontal Zone, seamount and southern stations

Additive modelling revealed that bioluminescent activity was significantly higher in the water column above the Faraday Seamount (SS53) compared to the reference station (SS54). Moreover, there was a significant difference in vertical distribution of luminescent organisms between both stations, with elevated concentrations of bioluminescence over the Faraday summit. These observations might be explained by a potential increase in biomass found over oceanic seamounts (Rogers, 1994). Upwelling and vertical mixing resulting from local currents that impinge upon the shoaling topography of underwater structures may favour productivity (White and Mohn, 2004). There are several mechanisms, including Taylor columns (Dower and Mackas, 1996) and larval retention (Mullineaux and Mills, 1997) that could explain high abundance over a seamount. Tokarev et al. (2003) surveyed the epipelagic zone above 11 seamounts in the Atlantic Ocean, and at the Dobroya, Slozhnaya and Mayskaya seamounts, similar to and near the Faraday Seamount, they reported high levels of epipelagic bioluminescence above the summits compared to the surrounding water column, with an increase in intensity up to 15 times higher than background levels.

In comparing the far southern station (SS52) with the reference station (SS54), the abundance of deep bioluminescence was significantly higher at the former. In terms of vertical distribution, SS52 exhibited lower abundance in the surface layers but increased levels in deeper layers, perhaps a result of a change in faunal composition of the zooplankton in subtropical waters.

4.4. North of the Front

Northwest of the CGFZ, smoother plots revealed significant differences in the distribution of pelagic bioluminescence between SS66 and SS76. When plotting temperature as a function of depth, it was found that apart from SS72 to SS76, all stations displayed a similar temperature–depth profile. The heterogeneity in the distribution of bioluminescence observed at those stations could be explained by the patchiness in the marine environment (Angel, 1993). Some pelagic organisms might form aggregations not only as a result from variations in abiotic factors but also as a response to other biotic parameters, such as feeding and reproduction (Methven et al., 2003) or predator–prey interactions (Widder et al., 1999).

4.5. Frontal Zone

Southeast of the CGFZ, relatively strong mesoscale variability was detectable at SS56–62 and the thermohaline structure at those stations revealed the presence of a warm-core anticyclonic eddy (Søiland et al., 2008). Additive modelling showed that, despite significantly different depth distributions, the abundance of pelagic bioluminescence was similar at SS56, 58 and 60. From hydrographic observations, SS62 was found to be located at the periphery of the eddy, which might explain the relatively lower abundance observed in its profile. The non-eddy

group (SS54 and SS64) also displayed similar abundance and different vertical distribution of bioluminescence. The presence of the eddy might have contributed to the enhancement of bioluminescent activity observed at SS56–62. The eddy body was characterized by a warm and salty core signature that extended vertically down from 0 to about 700 m (Søiland et al., 2008). As the water masses flow over the CGFZ there is a tendency for the formation of current-generated eddies that spin off from the NAC (Shoosmith et al., 2005). The core of anticyclonic oceanic eddies are typically zones of downwelling and therefore are nutrient-deficient (Sweeney et al., 2003). However, high primary production and pelagic biomass found in the cores of anticyclonic eddies have been reported previously (Woodward and Rees, 2001; Yebra et al., 2005). As the life span and stage of the present anticyclonic eddy could not be verified in this study, we were not able to ascertain whether the pelagic bioluminescent community measured in the Frontal Zone reflected the original biological state, or whether the organism developed during the eddy's journey to the present position. Different stages of eddy formation might harbour different pelagic communities, which could consequently affect the amount of pelagic bioluminescence in the mesoscale structure (Angel and Fasham, 1983; Olsen, 1991). The increased deep abundance observed at SS56, which was not caused by an anomaly in the contouring program, might be due to the time of sampling. This station was sampled at night and therefore diel vertical migration of bioluminescent mesopelagic organisms may be responsible for the high numbers of bioluminescent sources observed. However, the lack of enhanced bioluminescent activity at SS70, 76, 72 and 74 (North of the Front) which were also sampled at night, does not agree with this hypothesis.

The high concentrations of pelagic bioluminescence in this region might also be explained by the presence of the SPF. Oceanic fronts have been well documented as being sites of major upwelling and turbulence and have been found to harbour local proliferation and accumulation of zooplankton (Claustre et al., 1994), which might explain elevated levels of pelagic bioluminescence in the Frontal Zone. Moreover, several studies have shown increased bioluminescence in upwelling (Piontkovski et al., 1997) and hydrographic fronts (Cussatlegras et al., 2001).

Acknowledgements

The authors thank Dr. O.A. Bergstad for giving us the opportunity to carry out this work as part of the MAR-ECO project, a field project of the Census of Marine Life programme, and also the ship's company of the R.V. *G.O. Sars*. We are grateful to Drs. D. Bailey and T. Sutton for their critical reviews and constructive suggestions. We also thank Dr. A. Zuur for initial discussions of the statistical analyses. Finally, thanks to the anonymous reviewers who helped improve this manuscript. A. Heger was partially funded by the Luxembourgish Ministry of Culture, Higher Education and Research. N.J. King was supported by NERC studentship NER/S/A/2003/11190.

References

Angel, M.V., 1993. Biodiversity of the Pelagic Ocean. Conservation Biology 7 (4), 760–772.

Angel, M.V., Fasham, M.J.R., 1983. Eddies and biological processes. In: Robison, A.R. (Ed.), Eddies in Marine Science. Springer, Berlin Heidelberg.

Bower, A.S., Le Cann, B., Rossby, T., Zenk, W., Gould, J., Speer, K., Richardson, P.L., Prater, M.D., Zhang, H.-M., 2002. Directly measured mid-depth circulation in the northeastern North Atlantic Ocean. Nature 419, 603–607.

Bradner, H., Bartlett, M., Blackinton, G., Clem, J., Karl, D., Learned, J., Lewitus, A., Matsuno, S., O'Connor, D., Peatman, W., Reichle, M., Roos, C., Waters, J., Webster, M., Yarbrough, M., 1987. Bioluminescence profile in the deep Pacific Ocean. Deep-Sea Research I 34, 1831–1840.

Clarke, G.L., Hubbard, C.J., 1959. Quantitative records of luminescent flashing of oceanic animals at great depths. Limnology and Oceanography 4, 163–180.

Clarke, G.L., Kelly, M.G., 1965. Measurements of diurnal changes in bioluminescence from the sea surface to 2000 meters using a new photometric device. Limnology and Oceanography 10, R54–R66.

Claustre, H., Kerherve, P., Marty, J.C., Prieur, L., Videau, C., Hecq, J.-H., 1994. Phytoplankton dynamics associated with a geostrophic front: ecological and biogeochemical implications. Journal of Marine Research 52, 711–742.

Cleveland, W.S., 1993. Visualizing Data. Hobart Press, Summit, NJ, USA, 360pp.

Cussatlegras, A.-S., Geistdoerfer, P., Prieur, L., 2001. Planktonic bioluminescence measurements in the frontal zone of Almeira-Oran (Mediterranean Sea). Oceanologica Acta 24 (3), 239–250.

Dower, J.F., Mackas, D.L., 1996. "Seamount effects" in the zooplankton community near Cobb Seamount. Deep-Sea Research I 43 (6), 837–858.

Falkowski, P.G., Barber, R.T., Smetacek, V., 1998. Biogeochemical controls and feedbacks on ocean primary production. Science 281, 200–206.

Faraway, J.J., 2006. Linear Models with R. Chapman & Hall/CRC, Boca Raton, USA, 240pp.

Gillibrand, E.J.V., Jamieson, A.J., Bagley, P.M., Zuur, A.F., Priede, I.G., 2007. Seasonal development of a deep pelagic bioluminescent layer in the temperate NE Atlantic Ocean. Marine Ecology Progress Series 341, 37–44.

Hastie, T., Tibshirani, R.J., 1990. Generalized Additive Models. Chapman & Hall/CRC, Boca Raton, USA, 352pp.

Herring, P.J. (Ed.), 1990. Light and Life in the Sea. Cambridge University Press, Cambridge, UK, p. 365pp.

Herring, P.J., Widder, E.A., 2004. Bioluminescence of deep-sea coronate medusae (Cnidaria: Scyphozoa). Marine Biology 146, 39–51.

Mauritzen, C., Polzin, K.L., McCartney, M.S., Millard, R.C., West-Mack, D.E., 2002. Evidence in hydrography and density fine structure for enhanced vertical mixing over the Mid-Atlantic Ridge in the western Atlantic. Journal of Geophysical Research 107 (C10), 3147.

Methven, D.A., Schneider, D.C., Rose, G.A., 2003. Spatial pattern and patchiness during ontogeny: post-settled *Gadus morhua* from coastal Newfoundland. ICES Journal of Marine Science 60, 38–51.

Mullineaux, L.S., Mills, S.W., 1997. A test of the larval retention hypothesis in seamount-generated flows. Deep-Sea Research 44, 747–770.

Olsen, D.B., 1991. Rings in the ocean. Annual Review of Earth and Planetary Sciences 19, 283–311.

Piontkovski, S.A., Tokarev, Y.N., Bytukov, E.P., Williams, R., Kiefer, D.A., 1997. The bioluminescent field of the Atlantic Ocean. Marine Ecology Progress Series 156, 33–41.

Priede, I.G., Bagley, P.M., Way, S., Herring, P.J., Partridge, J.C., 2006. Bioluminescence in the deep sea: free-fall lander observations in Atlantic Ocean off Cape Verde. Deep-Sea Research I 53 (7), 1272–1283.

R Development Core Team, 2006. R: A Language and Environment for Statistical Computing. Vienna, Austria: R Foundation for Statistical Computing. ISBN 3-900051-07-0.

Rogers, A.D., 1994. The biology of seamounts. Advances in Marine Biology 30, 305–350.

Rossby, T., 1999. On gyre interactions. Deep-Sea Research II 46, 139–164.

Shoosmith, D.R., Richardson, P.L., Bower, A.S., Rossby, H.T., 2005. Discrete eddies in the northern North Atlantic as observed by looping RAFOS floats. Deep-Sea Research II 52, 627–650.

Søiland, H., Budgell, P., Knutsen, Ø., 2008. The physical oceanographic conditions along the Mid-Atlantic Ridge north of the Azores in June–July 2004. Deep-Sea Research II, this issue [doi:10.1016/j.dsr2.2007.09.015].

Stemmann, L., Hosia, A., Youngbluth, M.J., Søiland, H., Picheral, M., Gorsky, G., 2008. Vertical distribution (0–1000 m) of macrozooplankton, estimated using the Underwater Video Profiler, in different hydrographic regimes along the northern portion of the Mid-Atlantic Ridge. Deep-Sea Research II, this issue [doi:10.1016/j.dsr2.2007.09.019].

Sweeney, E.N., McGillicuddy Jr, D.J., Buesseler, K.O., 2003. Biogeochemical impacts due to mesoscale eddy activity in the Sargasso Sea as measured at the Bermuda Atlantic Time-series Study (BATS). Deep-Sea Research II 50, 3017–3039.

Sy, A., 1988. Investigation of large-scale circulation patterns in the central North Atlantic: the North Atlantic Current, the Azores Current, and the Mediterranean Water plume in the area of the Mid-Atlantic Ridge. Deep-Sea Research 35, 383–413.

Sy, A., Schauer, U., Meincke, J., 1992. The North Atlantic Current and its associated hydrographic structure above and eastwards of the Mid-Atlantic Ridge. Deep-Sea Research 39, 825–853.

Tokarev, Y.N., Bityukov, E.P., Williams, R., 2003. Influence of seamounts at the Atlantic Ocean on modification of the bioluminescence and plankton characteristics. Marine Ecological Journal 2 (1), 46–58.

Vinogradov, G.M., 2005. Vertical distribution of macroplankton at the Charlie–Gibbs Fracture Zone (North Atlantic), as observed from the manned submersible "Mir-1". Marine Biology 146, 325–331.

Webster, M.S., Roos, C.E., Roberts, A., Okada, A., Ohashi, Y., O'Connor, D., Mitiguy, R., Matsuno, S., March, R., Learned, J.G., Karl, D., Clem, J., Blackinton, G., Bradner, H., Babson, J., 1991. Mechanical stimulation of bioluminescence in the deep Pacific Ocean. Deep-Sea Research I 38, 201–217.

Wenneck, T. de Lange, Falkenhaug, T., Bergstad, O.A., 2008. Strategies, methods, and technologies adopted on the R.V. *G.O. Sars* MAR-ECO expedition to the Mid-Atlantic Ridge in 2004.

White, M., Mohn, C., 2004. Seamounts: a review of physical processes and their influence on seamount ecosystems. OASIS Report, University of Hamburg, 40pp.

Widder, E.A., Johnsen, S., 2000. 3D spatial point patterns of bioluminescent plankton: a map of the "minefield". Journal of Plankton Research 22 (3), 409–420.

Widder, E.A., Bernstein, S.A., Bracher, D.F., Case, J.F., Reisenbichler, K.R., Torres, J.J., Robison, B.H., 1989. Bioluminescence in the Monterey submarine canyon-image-analysis of video recordings from a midwater submersible. Marine Biology 100, 541–551.

Widder, E.A., Johnsen, S., Bernstein, S.A., Case, J.F., Neilson, D.J., 1999. Thin layers of bioluminescent copepods found at density discontinuities in the water column. Marine Biology 134, 429–437.

Wood, S.N., 2006. Generalised Additive Models: An Introduction with R. Chapman & Hall/CRC, Boca Raton, USA, 416pp.

Woodward, E.M.S., Rees, A.P., 2001. Nutrient distributions in an anticyclonic eddy in the northeast Atlantic Ocean, with reference to nanomolar ammonium concentrations. Deep-Sea Research II 48, 775–793.

Yebra, L., Almeida, C., Hernández-León, S., 2005. Vertical distribution of zooplankton and active flux across an anticyclonic eddy in the Canary Island waters. Deep-Sea Research I 52, 69–83.

Youngbluth, M.J., Sornes, T., Hosia, A., Stemmann, L., 2008. Vertical distribution and relative abundance of gelatinous zooplankton, *in situ* observations near the Mid-Atlantic Ridge. Deep-Sea Research II, this issue [doi:10.1016/j.dsr2.2007.10.002].

Zuur, A.F., Ieno, E.N., Smith, G.M., 2007. Analysing Ecological Data. Springer, New York Inc, 680pp.